Electronic Supplementary Information for

Hybrid organic–inorganic solar cells based on bismuth iodide and 1,6-hexanediammonium dication

*David M. Fabian and Shane Ardo**

Experimental

Preparation of $MAPbI_3$ and $HDABiI_5$ Solutions

All chemicals were used as received. Methylammonium iodide (MAI) was synthesized by slow addition of 6.5 mL of hydriodic acid (47% in water, stabilized with 1.5% hypophosphorous acid, Sigma-Aldrich) at room temperature to 6 mL of methylamine (40 wt. % in methanol, TCI America) at 0 °C with stirring, followed by continued stirring for 1 hr. MAI precipitate was recovered by evaporation of solvents at 50 °C under reduced pressure. To purify MAI, the precipitate was dissolved in ethanol, recrystallized from diethyl ether, and finally vacuum dried at 60 °C for 12 h. $MAPbI_3$ solution was then prepared by mixing MAI and PbI_2 (99%, Sigma-Aldrich) powders at approximately a 1:1 mole ratio, but with MAI in slight excess, in anhydrous *N*,*N*-dimethylformamide (DMF) at 70 °C inside a nitrogen-filled glovebox. The $MAPbI_3$ solution was stored in the glovebox until use, and was used within one week of preparation.

To synthesize 1,6-hexanediamine dihydriodide (HDA•2HI), 260.9 mg of 1,6-hexanediamine (98+%, Alfa Aesar) was dissolved in 5 mL methanol, and then 1 mL hydriodic acid was added slowly at 0 °C with stirring, followed by stirring for an additional 30 min. HDA•2HI precipitate was recovered by evaporation of solvents at 40 °C under reduced pressure. The precipitate was rinsed with diethyl ether, and vacuum dried at 60 °C for 12 h. $HDABiI_5$ solution was then prepared by mixing HDA•2HI and BiI_3 (99%, Sigma-Aldrich) powders at an approximately 1:1 mole ratio, but with HDA•2HI in slight excess, in anhydrous DMF at 70 °C inside a nitrogen-filled glovebox. The $HDABiI_5$ solution was stored in the glovebox until use, and was used within one week of preparation.

Materials Processing

All steps of materials deposition and device fabrication were performed in air with 40 – 60% relative humidity and as described below, unless noted otherwise. All thermal treatments

were performed using a hot plate. Fluorine-doped tin oxide coated glass (FTO) substrates were cleaned as follows: 1) sonicated in Alconox solution, 2) rinsed with deionized water, 3) rinsed with ethanol, 4) sonicated in ethanol, and 5) dried with nitrogen. To deposit the compact TiO_2 ($cTiO_2$) layer, a solution of titanium diisopropoxide bis(acetylacetonate) was pipetted onto a cleaned FTO substrate and then the substrate was spun at 2000 rpm (2000 rpm/s acceleration) for 60 s. The substrate was subsequently dried at 125 °C and then sintered at 550 °C for 30 min. Nanoparticles of TiO_2 were synthesized following a procedure by Ito et al.[1] The nanoparticle solution was further diluted in ethanol at a weight ratio of 1:3.5 TiO_2 nanoparticle solution:ethanol to make a mesoporous TiO_2 ($mTiO_2$) suspension. The $mTiO_2$ layer was deposited by spin coating this solution at 500 rpm (500 rpm/s acceleration) for 5 s and then 5000 rpm (5000 rpm/s acceleration) for 25 s, then dried at 125 °C, and then sintered at 550 °C for 30 min. A conventional method was used to deposit $MAPbI_3$ which was adapted from Kim et al.[2] and used for both $MAPbI_3$ and $HDABiI_5$. A filtered $MAPbI_3$ or $HDABiI_5$ solution in DMF was pipetted on top of the $mTiO_2$-coated FTO substrate and then the substrate was spun at 2000 rpm (2000 rpm/s acceleration) for 60 s, followed by rapid transfer to a hot plate that was preheated to 100 °C, and was subsequently annealed at 100 °C for 30 min.

Device Fabrication

Prior to the FTO cleaning step, a region of the FTO film was etched using 2 M HCl and Zn powder in order to prevent device shunting upon contact to the device top Au electrode. After performing the cleaning steps listed above (Materials Processing subsection), FTO substrates were further cleaned using an O_2 plasma treatment for 10 min. Following deposition of $HDABiI_5$ per the protocol described above (Materials Processing subsection), a 50 mM solution of 2,2',7,7'-tetrakis(*N*,*N*'-di-*p*-methoxyphenylamine)-9,9'-spirobifluorene (spiro-OMeTAD) dissolved in chlorobenzene with additives of 17.5 μL 4-*tert*-butylpyridine and 37.5 μL lithium bis(trifluoromethane)sulfonimide in acetonitrile (170 mg/mL) was deposited by spin coating at 3000 rpm (3000 rpm/s acceleration) for 60 s. The devices were then transferred into a nitrogen-filled glovebox and 80 nm of Au was thermally evaporated onto the devices at a base pressure of 5×10^{-6} mbar. The complete devices had an architecture of Au/spiro-OMeTAD/$HDABiI_5$/$mTiO_2$/$cTiO_2$/FTO.

Thermal stability tests

Thermal stability tests were performed in air for $MAPbI_3$ and $HDABiI_5$ thin films deposited on $mTiO_2/cTiO_2/FTO$ per the protocols above (Materials Processing and Device Fabrication subsections). Then, a transmission-mode ultraviolet–visible (UV–Vis) electronic absorption spectrum was acquired. The hot plate temperature was raised from the processing temperature (100 °C) in 20 °C increments and held at each temperature for 10 min, up to 200 °C. After each temperature treatment step, a UV–Vis absorption spectrum was acquired. For the $HDABiI_5$ thin film (Fig. 4a), the temperature was raised in a final step to 300 °C and held for 10 min, followed by acquisition of a UV–Vis absorption spectrum.

Characterization

UV–Vis absorption measurements were carried out using an Agilent Cary 60 spectrophotometer. Tauc plots were constructed from measured UV–Vis spectra. Spectra were baseline-subtracted for long-wavelength scattering, and bandgap energies were determined from best-fit lines of the data near the absorption onset. Scanning electron microscopy (SEM) images were acquired on a FEI Magellan 400L XHR. Grazing-incidence X-ray diffraction (XRD) data were collected using a Rigaku Smartlab diffractometer with Cu K_α radiation and in parallel-beam geometry. X-ray photoelectron spectroscopy (XPS) measurements and ultraviolet photoelectron spectroscopy (UPS) measurements were performed using a Kratos AXIS Supra photoelectron spectrometer using Al K_α radiation. For XPS measurements, two separate spots on the sample were evaluated to confirm matching peak intensities for binding energy scans of C 1s, N 1s, Bi 4f, I 3d, Ti 2p, and O 1s. UPS measurements were performed with an unfiltered He I (21.22 eV) gas discharge lamp, and Fermi edge calibration was performed with a sputter-cleaned Ag standard to ensure that all energies were referenced to a common Fermi level (0 eV). SEM, grazing-incidence XRD, XPS, and UPS work was performed in the UC Irvine Materials Research Institute (IMRI).

An ELH-type W–halogen lamp was used inside a nitrogen-filled glovebox as a source of simulated solar illumination. Before measurement of device *J–E* behavior and chronoamperometry behavior, the light intensity was roughly approximated to be 1 Sun using a calibrated Si photodiode (ThorLabs, Inc., FDS100) positioned at the location of the device. The integrated photocurrent of devices was determined from the product of the incident-photon-to-current efficiency (IPCE)

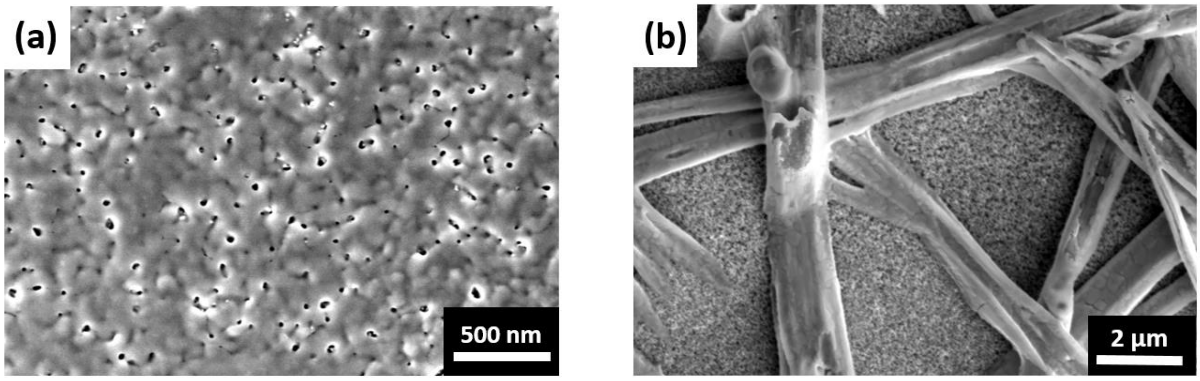

Figure S1. Top-view scanning electron microscopy image of (a) $HDABiI_5$ and (b) $MAPbI_3$ deposited on $mTiO_2/cTiO_2/FTO$. The overall surface coverage of $HDABiI_5$ on $mTiO_2$ is good compared to that of $MAPbI_3$ on $mTiO_2$.

values and the air mass 1.5 global (AM1.5G) solar photon flux spectrum at 1 Sun intensity; however, the simulated solar illumination for measurement of *J–E* behavior and chronoamperometry behavior was more accurately determined to be 0.8 Suns (i.e. the steady-state photocurrent density measured by the ELH lamp was 0.115 mA/cm^2, and the integrated photocurrent density measured by the IPCE setup was 0.143 mA/cm^2, and so 0.115 / 0.143 = 0.8). Cyclic voltammetry measurements (at a scan rate of 100 mV s^{-1}) and chronoamperometry measurements were performed using a Gamry Reference 600 Potentiostat. The diode quality factor of a device was measured by evaluating the dependence of the open-circuit photovoltage on light intensity. The light intensity was varied by adjusting the position of the lamp source with respect to the position of the tested device. The data were fit to the Shockley diode equation by the method of least squares and the diode quality factor was determined to be ~1.3. IPCE action spectra were determined using a Cornerstone 260 monochromator equipped with a 100 W APEX2 Xe arc lamp, and an NREL-calibrated Si solar cell as the reference.

Supplementary Figures and Associated Text

UPS Calculations

The work function and valence band maximum (VBM) of $HDABiI_5$ were measured by UPS to be –3.7 ± 0.1 eV and –5.6 ± 0.2 eV *versus* vacuum, respectively (Fig. S2). The work function was calculated by subtracting the He I radiation energy of 21.2 eV from the high-binding-energy cutoff at 17.5 eV (Fig. S2a): 17.5 (± 0.1) eV – 21.2 eV = –3.7 ± 0.1 eV *versus* vacuum. In a similar manner performed by Schulz et al. for a bare $MAPbI_3$ surface,[3] the low-energy tail of the

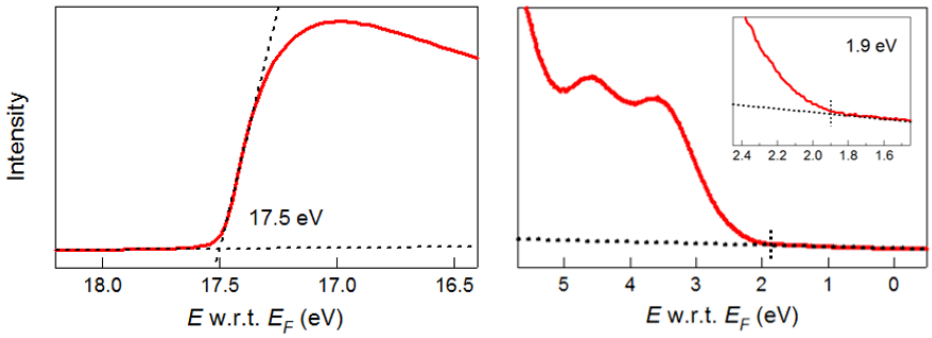

Figure S2. Ultraviolet photoemission spectra (He I) of $HDABiI_5$/FTO for direct determination of the work function (left) and valence-band maximum (right).

UPS spectrum was used to determine the position of the VBM as 1.9 ± 0.1 eV below the Fermi level, and therefore the VBM was calculated to be –3.7 (± 0.1) eV – 1.9 (± 0.1) eV = –5.6 ± 0.2 eV *versus* vacuum. Considering the calculated optical bandgap of ~2.1 eV (Fig. 1b and 1c), the conduction band minimum (CBM) was calculated to be –3.5 eV *versus* vacuum. This suggests that the Fermi level of $HDABiI_5$ lies close to the conduction band and therefore is n-type. The electronic band gap of the widely studied lead–halide-based perovskites has been shown to be 0.1 eV larger than the optical band gap,[3] and thus the CBM of $HDABiI_5$ may in fact lie at an energy closer to the vacuum level. An energy-level diagram is displayed as Fig. S3, where the calculated CBM (–3.5 eV) and VBM (–5.6 eV) are depicted. The CBM of TiO_2 (–4.21 eV *versus* vacuum) was taken from a report by Xu et al.,[4] and the VBM of spiro-OMeTAD (–5.15 eV *versus* vacuum) was taken from a report by Nguyen et al.[5] The spiro-OMeTAD/$HDABiI_5$ and $HDABiI_5$/TiO_2 interfaces are responsible for combined photovoltage losses of greater than 1 V, and so use of a

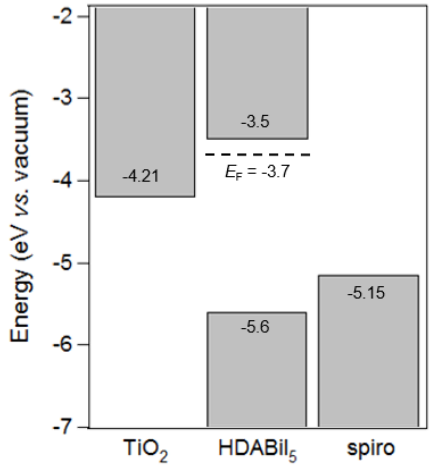

Figure S3. Energy-level diagram of spiro-OMeTAD/$HDABiI_5$/TiO_2, where the VBM of $HDABI_5$ was determined by UPS measurement.

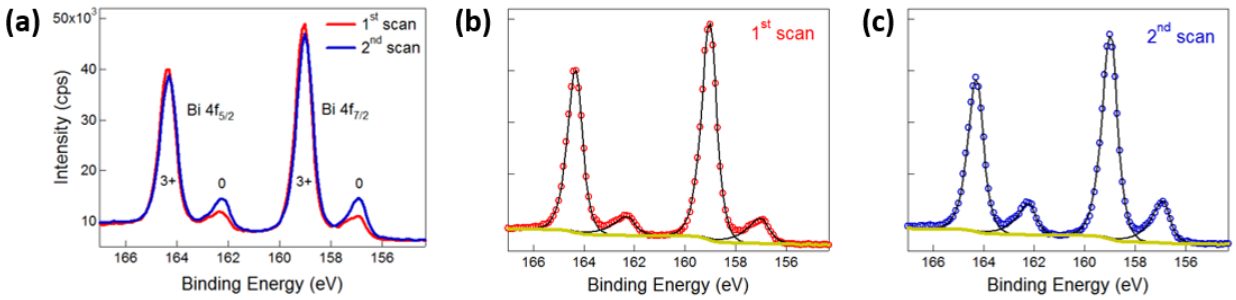

Figure S4. (a) Sequential X-ray photoelectron spectra of the Bi 4f region, which demonstrate increased signal attributed to Bi^0 compared to signal attributed to Bi^{3+} concomitant with longer exposure to Al K_α X-ray radiation. (b) First scan (red circles) and (c) second scan (blue circles) of the Bi 4f region, with Shirley backgrounds (gold curves) and peak fits (black curves) shown for clarity.

hole-transporting material with a more negative VBM and an electron-transporting material with a less negative CBM may result in a device with a larger photovoltage.

Explanation for XPS-induced Formation of Bi^0 Species

The first XPS Bi 4f region scan displayed in Fig. 2b is also displayed in Fig. S4 (red) and was the first scan acquired for the sample. A subsequent Bi 4f scan was acquired immediately afterward and is also shown in Fig. S4 (blue). For each scan, an emission current of 20 mA was used and two sweeps were performed. The data were analyzed using CasaXPS Processing Software. The peaks were fit to Gaussian–Lorentzian (80:20) curves, and percent concentration of Bi^0 was determined to be ~15% in the first scan and ~20% in the second scan. This suggests that some Bi^0 species formed as degradation during X-ray radiation, and that some Bi^0 was most likely present on the surface of the as-deposited $HDABiI_5$. No Bi^0 peaks could be resolved by grazing-incidence XRD, suggesting that any Bi^0 present at the surface of the as-deposited film likely existed as isolated atoms or small amorphous clusters.

XPS Calculations

Using CasaXPS Processing Software, approximate elemental composition was determined based on regions scans of $HDABiI_5/mTiO_2/cTiO_2/FTO$. To take into account the contribution of the Ti $2p_{1/2}$ peak that is overlapped by the Bi $4d_{3/2}$ peak, the overall peak area of Ti was approximated as the Ti $2p_{3/2}$ peak area multiplied by 1.5, because the ratio of the Ti $2p_{1/2}$ to Ti $2p_{3/2}$ area is expected to be 1:2 (Fig. S5b).[6] The percent composition of Ti was therefore determined to be 0.6 atom % (Table S1). Approximate percent elemental composition at the surface of

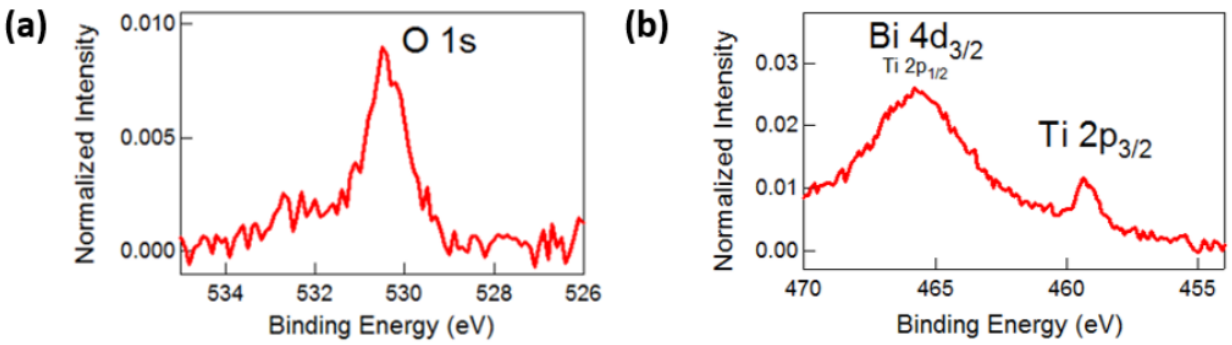

Figure S5. XPS region scans of (a) O 1s and (b) Ti 2p binding energies for $HDABiI_5/mTiO_2/cTiO_2/FTO$, where the intensities are normalized to the I $3d_{5/2}$ peak in Fig. 2b. Small peak intensities indicate near-complete coverage of $mTiO_2$ by $HDABiI_5$.

$HDABiI_5/mTiO_2/cTiO_2/FTO$ (Table S1), which was calculated based on region scans, indicates ~98% coating of $mTiO_2$ by $HDABiI_5$.

Table S1. Approximate percent surface elemental composition (excluding hydrogen) of $HDABiI_5/mTiO_2/cTiO_2/FTO$ calculated from XPS region scans.

Element	Composition (%)
Carbon	47.2
Iodine	31.1
Nitrogen	12.3
Bismuth	7.4
Oxygen	1.4
Titanium	0.6

References

(1) Ito, S.; Murakami, T. N.; Comte, P.; Liska, P.; Grätzel, C.; Nazeeruddin, M. K.; Grätzel, M. *Thin Solid Films* **2008**, *516*, 4613–4619.

(2) Kim, H.-S.; Lee, C.-R.; Im, J.-H.; Lee, K.-B.; Moehl, T.; Marchioro, A.; Moon, S.-J.; Humphry-Baker, R.; Yum, J.-H.; Moser, J. E.; Grätzel, M.; Park, N.-G. *Sci. Rep.* **2012**, *2*, 591.

(3) Schulz, P.; Edri, E.; Kirmayer, S.; Hodes, G.; Cahen, D.; Kahn, A. *Energy Environ. Sci.* **2014**, *7*, 1377–1381.

(4) Xu, Y.; Schoonen, M. A. A. *Am. Mineral.* **2000**, *85*, 543–556.

(5) Nguyen, W. H.; Bailie, C. D.; Unger, E. L.; McGehee, M. D. *J. Am. Chem. Soc.* **2014**, *136*, 10996–11001.

(6) Watts, J. F.; Wolstenholme, J. *An Introduction to Surface Analysis by XPS and AES*; 1st ed.; John Wiley & Sons Ltd.: Chichester, **2003**.